doi.org/10.26434/chemrxiv.12830384.v1

An Improved Route to Osmium(IV) Tetraaryl Complexes

Joseph Parr, Ralf Haiges, Michael Inkpen

Submitted date: 19/08/2020 • Posted date: 20/08/2020

Citation information: Parr, Joseph; Haiges, Ralf; Inkpen, Michael (2020): An Improved Route to Osmium(IV) Tetraaryl Complexes. ChemRxiv. Preprint. https://doi.org/10.26434/chemrxiv.12830384.v1

Air-stable, redox-active osmium(IV) tetraaryl complexes can be prepared in yields ≤76% from the novel precursor $(Oct_4N)_2[OsBr_6]$, facilitating the synthesis of $Os(mesityl)_4$ for the first time. This complex exhibits a distorted tetrahedral geometry and three reversible redox events including a 1+/2+ feature not previously observed in this family of materials.

File list (2)

An improved route to osmium(IV) tetraaryl complexes

Joseph M. Parr, Ralf Haiges, and Michael S. Inkpen*

Department of Chemistry, University of Southern California, Los Angeles, California 90089, United States

Email: inkpen@usc.edu

Abstract

Air-stable, redox-active osmium(IV) tetraaryl complexes can be prepared in yields ≤76% from the novel precursor $(Oct_4N)_2[OsBr_6]$, facilitating the synthesis of $Os(mesityl)_4$ for the first time. This complex exhibits a distorted tetrahedral geometry and three reversible redox events including a 1+/2+ feature not previously observed in this family of materials.

Homoleptic transition metal(IV) tetraaryl complexes, $M(aryl)_4$, are an underexplored class of organometallic materials with distinct electrochemical, magnetic, and optical properties resulting from their tetrahedral coordination geometry.[1] Os(IV)[2–4] and Ru(IV)[3–5] compounds with ortho-methylated σ-aryl ligands are particularly robust (consistent with a stable d^4 low-spin electronic configuration), where the methyl groups provide steric protection from decomposition pathways such as reductive elimination and *ortho*-hydrogen abstraction.[3] They can be purified using chromatography in air, and their aryl ligands can be chemically functionalized via different methods (including bromination,[6] Suzuki coupling,[6] and Friedel-Crafts acylation[7]). The osmium compounds have a particularly rich redox chemistry which facilitated the early isolation of a stable paramagnetic Os(V) complex.[8] However, $Os(aryl)_4$ complexes are often obtained in poor yields (typically ≤34%, see **SI, Table S2**) from reactions of aryl Grignard reagents with OsO_4 (aryl = 2-tolyl, 2,5-xylyl, 2,4-xylyl, 4-fluoro-2-tolyl, and phenyl). Given the high toxicity of OsO_4, and additional purification complications caused by the presence of monooxo(tetraaryl)osmium(VI)[9] and bisoxo(diaryl)osmium(VI)[9,10] side products (**Figure 1**, top), the development of new, high-yielding preparative approaches using alternative starting reagents is desirable.

In this work we report an improved synthetic route to osmium(IV) tetraaryl complexes starting from novel tetra-*n*-octylammonium hexahaloosmate(IV) precursors ($(Oct_4N)_2[OsX_6]$; X = Cl, Br; **Figure 1**, bottom); our approach can also be used to prepare ruthenium homologues from tetra-*n*-octylammonium hexachlororuthenate(IV). Reactions of the appropriate aryl Grignard reagent with $(Oct_4N)_2[OsBr_6]$ provide Os(2-tolyl)$_4$ (**Os1**) and Os(2,5-xylyl)$_4$ (**Os2**) in the highest yields reported for any $M(aryl)_4$ compound prepared to date (≥75%). Analogous reactions using mesitylmagnesium bromide provide Os(mesityl)$_4$ (**Os3**) in ≤21%, a previously inaccessible complex comprising sterically demanding and electron rich 2,6-dimethyl substituted aryl ligands. We unambiguously determine the structure of **Os2** and **Os3** via single-crystal X-ray diffraction (**Figure 2**) and explore the redox properties of **Os1-3** using solution electrochemistry (**Figure 3**).

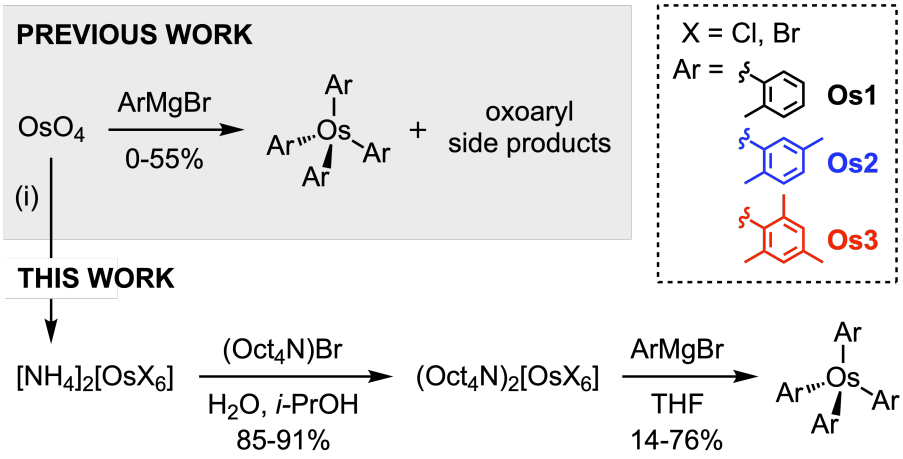

Figure 1. Synthetic routes to Os(aryl)$_4$ complexes from reactions of aryl Grignard reagents with OsO_4 (previous work, top) or $(Oct_4N)_2[OsX_6]$ (this work, bottom). Conditions: (i) HX, NH_4X (X = Cl, Br), ethanol (and $FeCl_2$ for X = Cl).[11,12] Use of $(Oct_4N)_2[OsX_6]$ avoids the formation of osmium(VI) oxoaryl side products, provides higher yields of Os(aryl)$_4$, and facilitates the formation of Os(mesityl)$_4$ (**Os3**) for the first time.

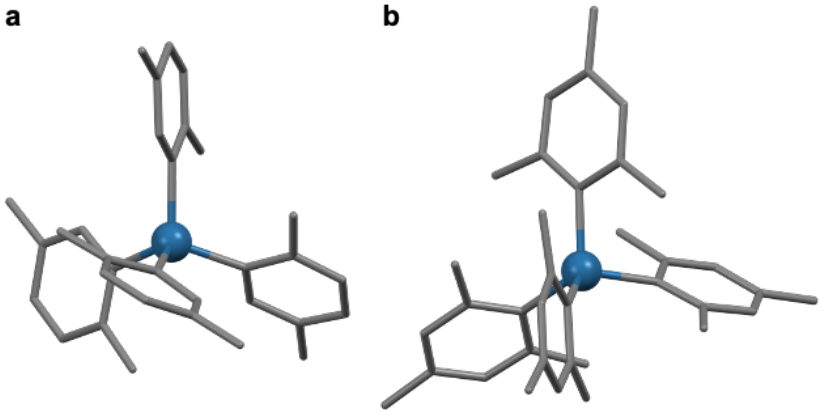

Figure 2. X-ray crystal structures of **(a) Os2** and **(b) Os3**. Hydrogen atoms are omitted for clarity (Os = teal, C = grey). Selected structural parameters are provided in **Table 1** and in the **SI, Table S7**, **S8**, and **S13**.

In developing this method, we considered approaches that might reduce or eliminate the formation of osmium(VI) oxoaryl side products. These are reported to originate from the incomplete substitution of OsO_4 rather than through air oxidation in solution or during chromatographic purification.[9] We reasoned that oxoaryl side products could be avoided simply by using alternative oxygen-free osmium precursors, and looked for inspiration from the materials used to prepare analogous ruthenium(IV) tetraaryl complexes. These include $(Et_4N)[RuCl_5(THF)]$,[4] $(Et_4N)[RuCl_5(MeCN)]$,[4] $Ru_2(\mu\text{-}O_2CMe)_4$,[4] $RuCl_3(tht)_3$,[5] and $Ru(acac)_3$[13,14] (tht = tetrahydrothiophene, acac = acetylacetonate). Unfortunately, yields of the Ru(aryl)$_4$

products are also low, and methods involving some of these precursors are reportedly difficult to reproduce (**SI, Table S1**).[4,5] Given that the use of multinuclear, Ru(II), or Ru(III) species also have the potential to increase the complexity of reactions,[4] and noting that the mononuclear pentachlororuthenate salts have not been utilized since the first synthetic reports of Ru(aryl)$_4$ species, we sought alternative easily accessible M(IV) compounds. Remarkably, several members of the family of $(NH_4)_2[MX_6]$ salts (M = Os, Ru; X = Cl, Br) are commercially available or readily synthesized using verified protocols,[11,12] but have not yet been explored as precursors to M(aryl)$_4$ compounds.

Our initial attempts to prepare Ru(2-tolyl)$_4$ (**Ru1**) by the addition of 6-8 equivalents of 2-tolylmagnesium bromide to $(NH_4)_2[RuCl_6]$ proved unsuccessful due to the low solubility of the metal salt in THF and diethyl ether (coordinating solvents commonly used for Grignard reactions). However, following cation exchange to increase solubility of the anion in common organic solvents, the analogous reaction using $(Oct_4N)_2[RuCl_6]$[15] provided **Ru1** in 35% yield (**SI, Figure S1**). This yield is comparable to those from previously reported routes (**SI, Table S1**). We readily adapted this cation exchange protocol to prepare the novel Os(IV) starting materials $(Oct_4N)_2[OsCl_6]$ and $(Oct_4N)_2[OsBr_6]$ in 85% and 91% yield, respectively (**Figure 1**, bottom). **Os1** (X = Cl, 30%; X = Br, 75%) and **Os2** (X = Cl, 44%; X = Br, 76%) could be isolated in high yields following reactions between these salts and the appropriate arylmagnesium bromide (see **SI, Table S2** for a summary of previous work). Further demonstrating the advantage of this approach, reaction of mesitylmagnesium bromide with $(Oct_4N)_2[OsX_6]$ provided the novel **Os3** complex as a green-black solid (X = Cl, 14%; X = Br, 21%). Previous attempts by others to prepare Os(aryl)$_4$ complexes with bulky 2,6-disubstituted aryl ligands from OsO_4, such as **Os3** or Os(2,6-xylyl)$_4$, resulted only in the formation of OsO_2(aryl)$_2$ complexes.[3,10,16] **Os1-3** and **Ru1** were worked up in air and purified by chromatography without any signs of decomposition.

The solid-state structures of **Os2** and **Os3** were determined by single-crystal X-ray diffraction and compared to analogous tetrahedral compounds (**Figure 2**, **Table 1** and **SI, Tables S7-S20**). While M-C bond lengths (**Os2** = 2.008(4) Å, **Os3** = 2.037(3) Å) appear to increase for Os(IV) compounds as the aryl ligands become more electron-donating (phenyl < 2-tolyl < 2,5-xylyl < cyclohexyl < mesityl; **Table 1**), the same trend is not observed for the Ru(IV) analogues. The range of angles between aryl planes does not appear to correlate with the number of ortho-substituents or the electronic character of the aryl ligand (**Table 1** and **SI, Table S7;** see **SI, Figure S2** for structural parameter

definitions). However, we note that **Os2** has the largest difference between minimum and maximum aryl plane angles for all compounds surveyed here (36.77°; **Table 1**).

Table 1. Selected average and calculated structural parameters for different compounds.

compound	M-C (Å) [a]	aryl plane range (°) [b]	*T*-value [c]	identifier [d]	reference
Os(mesityl)$_4$ (**Os3**)	2.037(3)	18.96	8.02	2024176	this work
Os(cyclohexyl)$_4$	2.029	-	5.18	1135690	[3]
Os(2-tolyl)$_4$ (**Os1**)	1.997	7.51	4.38	1135692	[3]
Os(4-Br-2,5-xylyl)$_4$	2.000(2)	24.87	1.60	164949	[6]
Os(phenyl)$_4$	1.995	24.40	1.32	1153940	[3]
Os(2,5-xylyl)$_4$ (**Os2**)	2.008(4)	36.77	1.11	2024175	this work
Ru(mesityl)$_4$ (**Ru3**)	2.01(1)	17.22	7.42	1191069	[5]
Ru(cyclohexyl)$_4$	2.019	-	4.02	1153943	[3]
Ru(2-tolyl)$_4$ (**Ru1**)	1.995	12.53	3.53	1161553	[4]
Ru(4-MeO-2-tolyl)$_4$	1.986	26.19	2.45	1032104	[13]
Ru(4-Br-2,5-xylyl)$_4$	1.984	24.97	2.17	1032108	[13]
Ru(2,4,5-trimethylphenyl)$_4$	1.985(10)	20.99	0.86	1510576	[14]
C(phenyl)$_4$	1.551	5.98	1.95	191149	[17]

[a] Average bond length, provided with pooled estimated standard deviations (ESDs) in parentheses for all structures with associated ESDs. M = Os, Ru, C. [b] Difference between minimum and maximum aryl plane angles. [c] *T*-value (tetrahedricity) = a measure of the mean absolute deviation of a set of C–M–C angles from their ideal tetrahedral values (109.5°). *T*-value = 0 indicates no deviation. Calculated using **Equation S1**. [d] CCDC Deposition Number.

To simplify comparisons of C-M-C angles we employ a "tetrahedricity"-value (*T*-value), the root-mean-square deviation of a set of C–M–C angles from their ideal tetrahedral values (109.5°). This is calculated for **Os1-3**, **Ru1**, and related compounds using **Equation S1**, where a *T*-value = 0 indicates no deviation. An analogous "octahedricity" metric has been utilized in the structural characterization of metal polypyridyl complexes,[18–20] and related analyses have been performed for coordination environments in solid-state materials.[21,22] We observe that *T*-values decrease in the order **M3** > M(cyclohexyl)$_4$ > **M1** for both series of Os and Ru compounds (**Table 1**), suggesting that a greater tetrahedral distortion is required to accommodate aryl ligands of increased steric bulk. This analysis supports the view that steric constraints due to 2,6-dimethyl substituents contribute to the lower synthetic yields of **Os3** compared to **Os2** and **Os1** (**SI, Table S2**), given that the four mesityl groups of **Os3** are arranged in

a particularly distorted tetrahedral geometry (T-value = 8.02, C-Os-C angles between 98.4-117.2°). In contrast, complexes with 2,5-xylyl ligands adopt a more ideal tetrahedral structure compared to **M1** and materials with simple phenyl substituents (**Table 1**). For example, **Os2** (T-value = 1.11, C-Os-C angles between 108.6-110.9°) is more tetrahedral than **Os1** (T-value = 4.38), Os(phenyl)$_4$ (T-value = 1.32), or C(phenyl)$_4$ (T-value = 1.95). In the **SI, Figure S3**, we present space-filling models that show the 2,6-dimethyl substituents of **Os3** provide additional steric shielding around the Os center compared with **Os1** and **Os2**. We hypothesize that 2,6-substituted aryl ligands may impart an increased chemical or electrochemical stability to such complexes, which have been shown to undergo rapid reactions with different Lewis bases.[23]

We studied the redox properties of **Os1-3** using cyclic voltammetry in CH_2Cl_2 with 0.1 M NBu_4PF_6 as the supporting electrolyte. The results are summarized in **Table 2** and **Table S21**, with representative overlaid cyclic voltammograms shown in **Figure 3**. Voltammograms for **Os3** at different scan rates are shown in **SI, Figure S4**. **Os1-3** exhibit two reversible, one-electron transfers ($i_{pa}/i_{pc} \approx 1$, $i_p \propto V_s^{1/2}$), in broad agreement with previous reports.[8,9] These 0/1+ and 1−/0 events have previously been assigned to the Os^{4+}/Os^{5+} and Os^{3+}/Os^{4+} redox couples, respectively. We observe an additional 1+/2+ oxidation event for **Os3** at +1.117 V which may be metal Os^{5+}/Os^{6+} or ligand-based. Using the equilibrium potentials for the 0/1+ feature of **Os1-3**, we find that Os(aryl)$_4$ complexes are approximately ~22 mV easier to oxidize for every methyl substituent added. This is compared to ~50 mV/methyl group for ferrocene analogues.[24] Using these values, we estimate the 0/1+ equilibrium potential of Os(2,3,4,5,6-pentamethylphenyl)$_4$ (**Os5**) to be around −0.02 mV vs. $[Cp_2Fe]^+/[Cp_2Fe]$, with a total range of ~350 mV between the mono-substituted and permethylated complexes (4-20 methyl substituents). This compares to ~500 mV between ferrocene and decamethylferrocene (0-10 methyl substituents).

Table 2. Selected electrochemical data for $Os(aryl)_4$ complexes.[a]

entry	compound	solvent	$E_{1/2}$ (V)				reference
			2−/1−	1−/0	0/1+	1+/2+	
1 [b]	$Os(2\text{-tolyl})_4$ (**Os1**)	THF	−2.47	−1.89	+0.41	-	[8]
2 [b]		CH_2Cl_2	-	−1.96	+0.33	-	[8]
3		CH_2Cl_2	-	−1.961	+0.326	-	this work
4 [c]	$Os(2,5\text{-xylyl})_4$ (**Os2**)	CH_2Cl_2	-	−1.48 [d]	+0.24	-	[9]
5		CH_2Cl_2	-	−2.008	+0.244	-	this work
6	$Os(mesityl)_4$ (**Os3**)	CH_2Cl_2	-	−2.028	+0.153	+1.117	this work

[a] Scan rate = 0.1 V s^{-1}; NBu_4PF_6 supporting electrolyte; working electrode: glassy carbon; reference electrode, counter electrode: Pt. Potentials measured with internal Cp^*_2Fe (−0.532 V vs $[Cp_2Fe]^+/[Cp_2Fe]$),[24] reported relative to $[Cp_2Fe]^+/[Cp_2Fe]$. See **SI, Table S22** for additional electrochemical data. [b] Scan rate = 0.05 V s^{-1}; working electrode: Pt; reference electrode: Ag; counter electrode: W. Potentials measured with internal Cp_2Fe. [c] Reference electrode: $Ag/AgNO_3$ (0.1 M in acetonitrile). Potentials measured with internal Cp_2Fe. [d] The reported potential of the 1−/0 redox event is significantly shifted compared to other measurements for these compounds.

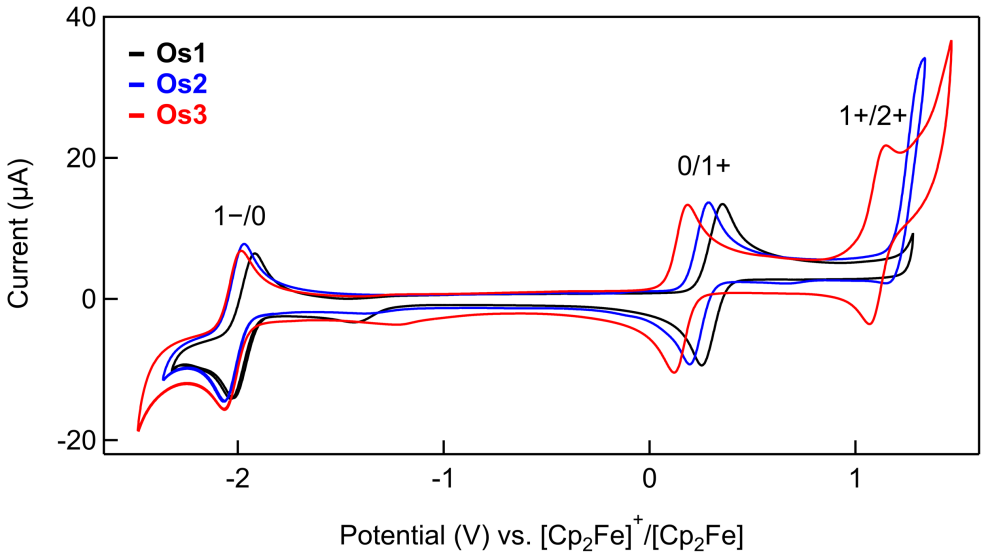

Figure 3. Overlaid cyclic voltammograms for $Os(2\text{-tolyl})_4$ (**Os1**, black), $Os(2,5\text{-xylyl})_4$ (**Os2**, blue), and $Os(mesityl)_4$ (**Os3**, red) in 0.1 M NBu_4PF_6–CH_2Cl_2. Potentials are reported relative to $FcH/[FcH]^+$, corrected for iR_u. Scan rate = 0.1 V s^{-1}. Redox features are shifted to cathodic potentials with increasing numbers of methyl substituents, and a second oxidation event is observed for **Os3**.

CONCLUSION

In conclusion, we have shown that synthetic yields of $Os(aryl)_4$ complexes can be significantly improved using the novel starting material $(Oct_4N)_2[OsBr_6]$, even

facilitating the preparation of previously inaccessible compounds such as **Os3**. $(Oct_4N)_2[OsBr_6]$ is relatively non-hazardous, straightforward to prepare, and convenient to handle, avoiding the direct use of volatile and toxic OsO_4 in reactions with aryl Grignard reagents. By quantifying the degree of tetrahedral distortion in these materials using a tetrahedricity metric, we show how their geometry is altered by varying the degree of substitution at the aryl ligands. Solution electrochemical studies of **Os1-3** suggest that the redox potentials of such compounds, with 20 possible substituent positions, can be precisely and systematically tuned. It is hoped that this study will help increase the utility of this fascinating family of complexes in established and emerging areas of molecular materials science.

ASSOCIATED CONTENT

Electronic Supplementary Information (ESI) available: Experimental procedures, characterization data (^{1}H and ^{13}C{^{1}H} NMR, high-resolution mass spectrometry or elemental analysis) for all new compounds, X-ray crystal structure data for **Os2** and **Os3,** and solution electrochemical data for **Os1-3**. CCDC 2024175, 2024176.

AUTHOR INFORMATION

Corresponding Author

Michael S. Inkpen – Email: inkpen@usc.edu

Notes

The authors declare no competing interests.

ACKNOWLEDGEMENTS

This work was supported by University of Southern California (USC) startup funds. J.M.P. is grateful for support from a USC Wrigley Institute for Environmental Studies Norma and Jerol Sonosky Environmental Sustainability Graduate Summer Fellowship. The authors thank John Arnold (University of California, Berkeley) for valuable discussions.

REFERENCES

1. Koschmieder, S. U. & Wilkinson, G. Homoleptic and related aryls of transition metals. *Polyhedron* **10**, 135–173 (1991).
2. Tooze, R. P., Stavropoulos, P., Motevalli, M., Hursthouse, M. B. & Wilkinson, G.

Synthesis and x-ray crystal structures of the first tetrahedral osmium(IV) compounds, tetrakis(cyclohexyl)osmium(IV) and tetrakis(o-methylphenyl)osmium(IV). *J. Chem. Soc. Chem. Commun.* **0**, 1139–1140 (1985).

3. Stavropoulos, P., Savage, P. D., Tooze, R. P., Wilkinson, G., Hussain, B., Motevalli, M. & Hursthouse, M. B. The synthesis and X-ray crystal structures of homoleptic tetrahedral aryls of osmium(IV) and of cyclohexyls of ruthenium(IV), osmium(IV), and chromium(IV). *J. Chem. Soc. Dalt. Trans.* 557–562 (1987).
4. Savage, P. D., Wilkinson, G., Motevalli, M. & Hursthouse, M. B. Synthesis of homoleptic tetrahedral aryls of rhenium(IV) and ruthenium(IV). X-Ray crystal structures of tetrakis(o-methylphenyl)rhenium(IV), tetrakis(o-methylphenyl)oxorhenium(VI), and tetrakis(o-methylphenyl)-ruthenium(IV). *J. Chem. Soc., Dalt. Trans.* 669–673 (1988) doi:10.1039/dt9880000669.
5. Hay-Motherwell, R., Wilkinson, G., Hussain-Bates, B. & Hurthouse, M. Homoleptic Mesityls of lridium(lw/,v) and Ruthenium(lv,v). *Dalton Trans.* 3477–3482 (1992).
6. Lau, M. K., Zhang, Q. F., Chim, J. L. C., Wong, W. T. & Leung, W. H. Direct functionalisation of σ-aryl ligands: Preparation of homoleptic functionalised aryls of osmium(IV). *Chem. Commun.* **1**, 1478–1479 (2001).
7. Savage, P. D. Organometallic Compounds of Rhenium and the Platinum Group Metals. (Ph.D. thesis, Imperial College of Science & Technology, 1987).
8. Arnold, J., Wilkinson, G., Hussain, B. & Hursthouse, M. B. Redox chemistry of the homoleptic aryl Os(2-MeC6H4)4: synthesis and characterization of the first osmium(V) organometallic [Os(2-MeC6H4)4][CF3SO3]. *J. Chem. Soc. Chem. Commun.* 1349–1350 (1988) doi:10.1039/c39880001349.
9. Lau, M.-K., Chim, J. L., Wong, W.-T., Williams, I. D. & Leung, W.-H. Synthesis and molecular structures of monooxo aryl complexes of osmium(VI). *Can. J. Chem.* **79**, 607–612 (2001).
10. Stravropoulos, P., Edwards, P. G., Behling, T., Wilkinson, G., Motevalli, M. & Hursthouse, M. B. Oxoaryls of rhenium-(V) and -(VI) and osmium(VI). X-Ray crystal structures of dimesityldioxorhenium(VI), tetramesityloxorhenium(VI), and dimesityldioxoosmium(VI). *J. Chem. Soc. Dalt. Trans.* 169–175 (1987) doi:10.1039/DT9870000169.
11. Dwyer, F. P., Hogarth, J. W. & Rhoda, R. N. Ammonium Hexachloroosmate (IV). *Inorg. Synth.* **5**, 206–207 (1957).
12. Dwyer, F. P., Hogarth, J. W. & Rhoda, R. N. Ammonium Hexabromoosmate (IV).

Inorg. Synth. **5**, 204–206 (1957).

13. So, S. C., Cheung, W. M., Wang, G. C., Kwan Huang, E., Lau, M. K., Zhang, Q. F., Sung, H. H. Y., Williams, I. D. & Leung, W. H. Migratory insertion and reductive coupling of tetraarylruthenium(IV) complexes. *Organometallics* **33**, 4497–4502 (2014).
14. Wang, C.-J., Wu, X.-L., Ma, X.-F., Jia, A.-Q. & Zhang, Q.-F. Synthesis and crystal structure of a new homoleptic tetraarylruthenium(IV) complex Ru(2,4,5-Me3C6H2)4. *Z. Naturforsch* **72**, 523–525 (2017).
15. Rodriguez, J. R., Félix, R. M., Reynoso, E. A., Fuentes Moyado, S. & Alonso-Núñez, G. Coordination complex synthesis of noble metals in the preparation of nanoparticles supported on MWCNTs used as electrocatalysts. *Inorganica Chim. Acta* **406**, 138–145 (2013).
16. Longley, C. J., Savage, P. D., Wilkinson, G., Hussain, B. & Hurthouse, M. Alkylimido and oxo aryls of rhenium. X-ray structures of (BuittN)2ReCl2(o-MeC6H4) and MO2(2,6-Me2C6H3)2, M = Re and Os. *Polyhedron* **7**, 1079–88 (1988).
17. Knop, O., Rankin, K. N., Cameron, T. S. & Boyd, R. J. Crystal chemistry of tetraradial species. Part 10. Tilting at windmills: Conformations of the tetraphenyl species ZPh40, ±1 (Z = B, C, N)1. *Can. J. Chem.* **80**, 1351–1366 (2002).
18. Brown, C. M., Arsenault, N. E., Cross, T. N. K., Hean, D., Xu, Z. & Wolf, M. O. Structural, electrochemical and photophysical behavior of Ru(ii) complexes with large bite angle sulfur-bridged terpyridyl ligands. *Inorg. Chem. Front.* **7**, 117–127 (2020).
19. Österman, T., Abrahamsson, M., Becker, H.-C., Hammarström, L. & Persson, P. Influence of Triplet State Multidimensionality on Excited State Lifetimes of Bis-tridentate RuII Complexes: A Computational Study. *J. Phys. Chem. A* **116**, 1041–1050 (2012).
20. Lundqvist, M. J. Quantum Chemical Modeling of Dye-Sensitized Titanium Dioxide : Ruthenium Polypyridyl and Perylene Dyes, TiO2 Nanoparticles, and Their Interfaces. (Ph.D. thesis, Uppsala University, 2006).
21. Hiwatari, Y., Saito, T. & Ueda, A. Structural characterization of soft-core and hard-core glasses by Delaunay tessellation. *J. Chem. Phys.* **81**, 6044–6050 (1984).
22. Medvedev, N. N. & Naberukhin, Y. I. Shape of the delaunay simplices in dense random packings of hard and soft spheres. *J. Non. Cryst. Solids* **94**, 402–406 (1987).
23. Arnold, J., Wilkinson, G., Hussain, B. & Hursthouse, M. B. Reactivity of the homoleptic osmium aryl Os(2-MeC6H4)4: ligand-induced reductive coupling, .sigma.-

to .pi.-rearrangement, and ortho-hydrogen activation. *Organometallics* **8**, 1362–1369 (1989).

24. Noviandri, I., Brown, K. N., Fleming, D. S., Gulyas, P. T., Lay, P. A., Masters, A. F. & Phillips, L. The Decamethylferrocenium/Decamethylferrocene Redox Couple: A Superior Redox Standard to the Ferrocenium/Ferrocene Redox Couple for Studying Solvent Effects on the Thermodynamics of Electron Transfer. *J. Phys. Chem. B* **103**, 6713–6722 (1999).

Supplementary Information

An improved route to osmium(IV) tetraaryl complexes

Joseph M. Parr, Ralf Haiges, and Michael S. Inkpen*

Department of Chemistry, University of Southern California, Los Angeles, California, 90089, United States

E-mail: inkpen@usc.edu

Contents

1. Synthetic Details

All manipulations were carried out in oven-dried glassware under a nitrogen atmosphere using standard Schlenk line techniques. No special precautions were taken to exclude air or moisture during workup unless otherwise stated. Tetrahydrofuran and dichloromethane were sparged with nitrogen and dried using a two-column solvent purification system packed with alumina (Pure Process Technologies, Nashua, NH, USA). Grignard reagents were commercially available or prepared according to the general method described here, and titrated using a salicylaldehyde phenylhydrazone indicator to determine their concentration prior to use.[1] Automated flash chromatography was performed using a Pure C-850 FlashPrep chromatography system and FlashPure EcoFlex flash cartridges (BUCHI Corporation, New Castle, DE, USA; irregular 40-63 μm silica). $(Oct_4N)_2[RuCl_6]$[2] was prepared using established literature procedures. $(NH_4)_2[OsCl_6]$[3] and $(NH_4)_2[OsBr_6]$[4] were prepared using established literature procedures or purchased from commercial vendors. All other chemical reagents were purchased from commercial suppliers and used without further purification.

^1H and $^{13}C\{^1H\}$ NMR were recorded at room temperature on Varian VNMRS 500 (500 MHz) or Varian 400MR (400 MHz) NMR spectrometers. ^1H NMR data recorded in $CDCl_3$ and CD_2Cl_2 is referenced to residual internal $CHCl_3$ (δ 7.26) and $CDHCl_2$ (δ 5.32) solvent signals.[5] $^{13}C\{^1H\}$ NMR data recorded in $CDCl_3$ and CD_2Cl_2 is referenced to internal $CDCl_3$ (δ 77.16) and CD_2Cl_2 (δ 53.84) signals.[5] Mass spectrometry analyses were performed on an Agilent 6545 QTOF mass spectrometer fitted with an atmospheric pressure electrospray ionization source (Dual AJS ESI). Microanalyses were carried out using a Thermo Flash 2000 CHNS Combustion Analyzer, configured for %CHNS. Electrochemical measurements were performed under an argon atmosphere using a CHI760E bipotentiostat (CH Instruments, Austin, TX, USA) with anhydrous, nitrogen-sparged 0.1 M tetrabutylammonium hexafluorophosphate (NBu_4PF_6) dichloromethane solutions. We used a glassy carbon disc working electrode (Ø = 3 mm, CH Instruments), with Pt wire reference and counter electrodes. Prior to use, glassy carbon electrodes were mechanically polished using an alumina slurry, and Pt wires were cleaned by annealing in an oxyhydrogen flame. Analyte solutions were between 0.1-1 mM. Potentials are reported relative to $[Cp_2Fe]^+/[Cp_2Fe]$, measured against internal Cp_2Fe or Cp^*_2Fe references, as appropriate.

General Synthesis of $(Oct_4N)_2[OsX_6]$ Complexes (X = Cl, Br)

This method is adapted from the synthesis of $(Oct_4N)_2[RuCl_6]$.[2] A solution of tetra-*n*-octylammonium bromide (2 mmol) in 2-propanol (50 mL) was added to aqueous solution of $(NH_4)_2[OsX_6]$ (1 mmol) in deionized water (45 mL). After 1 h, deionized water (10 mL) was added and the precipitate collected via filtration in air. The solid was rinsed with deionized water (3 x 20 mL) and dried under vacuum overnight.

$(Oct_4N)_2[OsCl_6]$

From tetra-*n*-octylammonium bromide (1.470 g, 2.68 mmol), 2-propanol (50 mL), $(NH_4)_2[OsCl_6]$ (0.577 g, 1.34 mmol), and deionized water (45 mL), 1.521 g of a yellow powder was obtained (85% yield). ^{1}H NMR ($CDCl_3$, 500 MHz): δ (ppm) 0.87 (t, 12H, J = 6.8 Hz), 1.21-1.33 (m, 24H), 1.37 (m, 8H), 1.49 (m, 8H), 1.77 (m, 8H), 3.23 (m, 8H).^{13}C{^{1}H} NMR ($CDCl_3$, 125 MHz): δ (ppm) 13.83, 22.38, 24.30, 27.56, 28.88, 29.38, 31.52, 69.04. Anal. Calc. for $C_{64}H_{136}N_2Cl_6Os$: C, 57.59; N, 2.10; H, 10.27%. Found: C, 57.64; N, 2.04; H, 10.22%.

$(Oct_4N)_2[OsBr_6]$

From tetra-*n*-octylammonium bromide (1.390 g, 2.54 mmol), 2-propanol (60 mL), $(NH_4)_2[OsBr_6]$ (0.935 g, 1.27 mmol), and deionized water (50 mL), 1.860 g of a red-brown powder was obtained (91% yield). ^{1}H NMR ($CDCl_3$, 500 MHz): δ (ppm) 0.87 (t, 12H, J = 5.7 Hz), 1.22-1.35 (m, 24H), 1.39 (m, 8H), 1.50 (m, 8H), 1.77 (m, 8H), 3.22 (m, 8H). ^{13}C{^{1}H} NMR ($CDCl_3$, 125 MHz): δ (ppm) 13.38, 21.92, 24.40, 27.76, 28.45, 29.08, 31.09, 69.70. HR-MS (ESI/Q-TOF) *m/z*: 466.5357 ($[Oct_4N]^+$ calc. for $C_{32}H_{68}N$: 466.5352), 665.4701 ($[OsBr_6]^-$ calc. for $OsBr_6$: 665.4715).

General Synthesis of Aryl Grignard Reagents

Magnesium turnings (15 mmol) were mechanically stirred overnight under nitrogen in a 3-neck round-bottomed flask connected to a reflux condenser. THF (5 mL) and 1,2-dibromoethane (0.2 mL) were added, whereby a solution containing the appropriate aryl bromide (5 mmol) in THF (10 mL) was added dropwise to the stirred mixture. This was maintained at a gentle reflux for 10 min using a heat gun. The flask was then immersed in an oil bath and heated at reflux for an additional 1 h. After cooling to room temperature, the solution was filtered via cannula then titrated (approximate yields 60-85%, based on concentration and volume of acquired Grignard reagent).[1]

General Synthesis of M(aryl)$_4$ Complexes from $(Oct_4N)_2[MX_6]$ (M = Os, Ru; X = Cl, Br)

A solution of the appropriate aryl Grignard reagent in THF (1.8 mmol) was added dropwise to a stirred suspension of $(Oct_4N)_2[MX_6]$ (0.3 mmol) in THF (10 mL). The mixture was stirred at room temperature for 2 h, then nitrogen-sparged methanol (1 mL) was added. The solvent was removed *in vacuo*. The resulting solid was dissolved in CH_2Cl_2, packed onto Celite and purified by automated flash chromatography in air (silica; hexanes). Where necessary, M(aryl)$_4$ compounds were further purified by sublimation to remove grease impurities.

*Os(2-tolyl)$_4$ (**Os1**)*

From $(Oct_4N)_2[OsCl_6]$: Using a solution of 2-tolylmagnesium bromide in THF (0.66 mL, 0.9 M, 0.60 mmol), $(Oct_4N)_2[OsCl_6]$ (0.113 g, 0.085 mmol), and THF (10 mL), a black powder was obtained (0.014 g, 30%). From $(Oct_4N)_2[OsBr_6]$: Using a solution of 2-tolylmagnesium bromide in THF (2.40 mL, 0.9 M, 2.16 mmol), $(Oct_4N)_2[OsBr_6]$ (0.490 g, 0.3 mmol), and THF (10 mL), a black powder was obtained (0.124 g, 75%). ^{1}H NMR ($CDCl_3$, 500 MHz): δ (ppm) 2.30 (s, 12H), 6.79 (m, 8H), 6.94 (m, 8H). HR-MS (ESI/Q-TOF) *m/z*: 556.1839 ($[M]^+$ calc. for $C_{28}H_{28}Os$: 556.1806).

*Os(2,5-xylyl)$_4$ (**Os2**)*

From $(Oct_4N)_2[OsCl_6]$: Using a solution of 2,5-xylylmagnesium bromide in THF (0.55 mL, 1.04 M, 0.57 mmol), $(Oct_4N)_2[OsCl_6]$ (0.108 g, 0.08 mmol), and THF (10 mL), a black powder was obtained (0.022 g, 44%). From $(Oct_4N)_2[OsBr_6]$: Using a solution of 2,5-xylylmagnesium bromide in THF (0.46 mL, 1.04 M, 0.48 mmol), $(Oct_4N)_2[OsBr_6]$ (0.216 g, 0.08 mmol), and THF (10 mL), a black powder was obtained (0.083 g, 76%). Crystals suitable for X-ray diffraction were grown by cooling a solution of **Os2** in *n*-hexane to −20°C (red-brown plate-like crystals). ^{1}H NMR ($CDCl_3$, 500 MHz): δ (ppm) 2.22 (s, 12H), 2.27 (s, 12H), 6.58 (d, 4H, J = 7.5 Hz), 6.67 (d, 4H, J = 7.5 Hz), 6.70 (s, 4H). HR-MS (ESI/Q-TOF) *m/z*: 612.2433 ($[M]^+$ calc. for $C_{32}H_{36}Os$: 612.2432).

From OsO_4: A solution of 2,5-xylylmagnesium bromide in THF (14 ml, 0.5 M, 7 mmol) was added dropwise to a stirred suspension of OsO_4 (0.250g, 0.98 mmol) in THF (10 ml) at −78°C under nitrogen. The resulting reddish-brown mixture was allowed to warm to room temperature and stirred for 2 h, then nitrogen-sparged methanol (1 mL) was added. The solvent was removed *in vacuo,* with the crude product consisting of a mixture of **Os2** and OsO(2,5-xylyl)$_4$ in approximate 2:1 ratio. The resulting solid was dissolved in hexanes, packed onto Celite and

purified by automated flash chromatography in air (silica; hexanes). **Os2** was obtained as a black solid (0.038 g, 6%).

*Os(mesityl)$_4$ (**Os3**)*

From $(Oct_4N)_2[OsCl_6]$: Using a solution of mesitylmagnesium bromide in THF (0.62 mL, 1.0 M, 0.62 mmol), $(Oct_4N)_2[OsCl_6]$ (0.118 g, 0.09 mmol), and THF (10 mL), a green-black powder was obtained (0.008 g, 14%). From $(Oct_4N)_2[OsBr_6]$: Using a solution of mesitylmagnesium bromide in THF (2.21 mL, 1.0 M, 2.21 mmol), $(Oct_4N)_2[OsBr_6]$ (0.505 g, 0.316 mmol), and THF (10 mL), a green-black powder was obtained (0.045 g, 21%). Crystals suitable for X-ray diffraction were grown by cooling a solution of **Os3** in *n*-hexane to −20°C (green-black needles). A sample of analytical purity was obtained by sublimation at 120°C under reduced pressure (~0.10 Torr). ^{1}H NMR ($CDCl_3$, 500 MHz): δ (ppm) 2.33 (s, 24H), 2.54 (s, 12H), 7.00 (s, 8H). $^{13}C\{^1H\}$ NMR ($CDCl_3$, 125 MHz): δ (ppm) 20.33, 28.68, 29.86, 123.30, 127.74, 141.23, 146.58. HR-MS (ESI/Q-TOF) *m/z*: 668.3039 ($[M]^+$ calc. for $C_{36}H_{44}Os$: 668.3058).

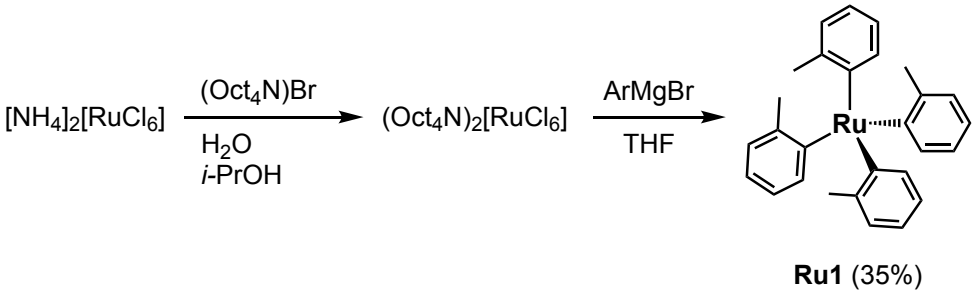

Figure S1. Synthetic route to **Ru1**.

*Ru(2-tolyl)$_4$ (**Ru1**)*

From $(Oct_4N)_2[RuCl_6]$: Using a solution of 2-tolylmagnesium bromide in THF (4.75 mL, 0.9 M, 4.27 mmol), $(Oct_4N)_2[RuCl_6]$ (0.253 g, 0.21 mmol), and THF (10 mL), a red-brown powder was obtained (0.034 g, 35%). ^{1}H NMR ($CDCl_3$, 500 MHz): δ (ppm) 2.13 (s, 12H), 6.90 (d, 4H, J = 5.8 Hz), 7.00 (m, 8H), 7.20 (d, 4H, J = 6.2 Hz). HR-MS (ESI/Q-TOF) *m/z*: 466.1232 ($[M]^+$ calc. for $C_{28}H_{28}Ru$: 466.1234).

2. Overview of Previous Synthetic Routes

Table S1. Selected reaction parameters for the synthesis of Ru(aryl)$_4$ complexes.

compound	metal salt	yield (%)	reference
Ru(2-tolyl)$_4$ (**Ru1**)	Ru$_2$(μ-O$_2$CMe)$_4$	24	[6]
	(NEt$_4$)[RuCl$_5$(MeCN)]	34	[6]
	(NEt$_4$)[RuCl$_5$(THF)]	48	[6]
	[Oct$_4$N]$_2$[RuCl$_6$]	35	this work
Ru(2,4,5-trimethylphenyl)$_4$	Ru(acac)$_3$	37	[7]
Ru(2,5-xylyl)$_4$ (**Ru2**)	Ru(acac)$_3$	34	[8]
Ru(4-MeO-2-tolyl)$_4$	Ru(acac)$_3$	29	[8]
Ru(2,6-xylyl)$_4$	(Et$_4$N)[RuCl$_5$(MeCN)]	13	[6]
	(Et$_4$N)[RuCl$_5$(THF)]	21	[6]
Ru(mesityl)$_4$ (**Ru3**)	Ru$_2$(O$_2$CMe)$_4$	21	[6]
	RuCl$_3$(tht)$_3$	18	[9]
Ru(p-*t*-butylphenyl)$_4$	(Et$_4$N)[RuCl$_5$(THF)]	20	[6]

Table S2. Selected reaction parameters for the synthesis of Os(aryl)$_4$ complexes.

M(aryl)$_4$	metal precursor	yield (%)	reference
Os(2-tolyl)$_4$ (**Os1**)	OsO$_4$	27	[10]
		55 [a]	[11]
	[N(Oct)$_4$]$_2$[OsCl$_6$]	30	this work
	[N(Oct)$_4$]$_2$[OsBr$_6$]	75	this work
Os(2,5-xylyl)$_4$ (**Os2**)	OsO$_4$	34	[12]
		6	this work
	[N(Oct)$_4$]$_2$[OsCl$_6$]	44	this work
	[N(Oct)$_4$]$_2$[OsBr$_6$]	76	this work
Os(mesityl)$_4$ (**Os3**)	OsO$_4$	- [b]	[13]
	[N(Oct)$_4$]$_2$[OsCl$_6$]	14	this work
	[N(Oct)$_4$]$_2$[OsBr$_6$]	21	this work
Os(2,4-xylyl)$_4$	OsO$_4$	50 [a]	[11]
Os(4-fluoro-2-tolyl)$_4$	OsO$_4$	34	[11]
Os(phenyl)$_4$ [c]	OsO$_4$	24	[14]

[a] Attempts by us and others[12] failed to reproduce yields ≥50% following the reported methods. [b] Reported attempts resulted only in isolation of oxoaryl osmium(VI) complexes.[13] This was also observed for structurally similar 2,6-dimethylated aryls such as 2,6-xylyl,[15] 2,3,5,6-tetramethylphenyl,[16] and 2,4,6-triisopropylphenyl ligands.[16] [c] Slowly decomposes over several days.[17]

3. X-Ray Crystallography

X-ray intensity data were collected at 100 K on a Bruker APEX DUO 3-circle platform diffractometer, equipped with an APEX II CCD detector, using MoKα radiation (λ = 0.71073 Å, TRIUMPH curved-crystal monochromator) from a fine-focus tube. The structures were solved by intrinsic phasing and refined on F^2 using the Bruker SHELXTL Software Package and ShelXle.[18–21] All non-hydrogen atoms were refined anisotropically. Further crystallographic details can be obtained from the Cambridge Crystallographic Data Centre (CCDC, 12 Union Road, Cambridge, CB2 1EZ, UK (Fax: (+44) 1223–336–033; e-mail: deposit@ccdc.cam.ac.uk) on quoting the deposition no. CCDC 2024175, 2024176.

Table S3. Sample and crystal data for **Os2**.

Chemical formula	$C_{32}H_{36}Os$	
Formula weight	610.81 g/mol	
Temperature	100(2) K	
Wavelength	0.71073 Å	
Crystal size	0.022 x 0.167 x 0.187 mm	
Crystal habit	dark red plate	
Crystal system	monoclinic	
Space group	C 1 c 1	
Unit cell dimensions	a = 12.9059(19) Å	α = 90°
	b = 12.9355(18) Å	β = 98.736(2)°
	c = 15.837(2) Å	γ = 90°
Volume	2613.2(7) $Å^3$	
Z	4	
Density (calculated)	1.553 g/cm^3	
Absorption coefficient	4.897 mm^{-1}	
F(000)	1216	

Table S4. Data collection and structure refinement for **Os2**.

Diffractometer	Bruker APEX DUO
Radiation source	fine-focus tube (MoKα , λ = 0.71073 Å)
Theta range for data collection	2.24 to 30.52°
Index ranges	-18<=h<=18, -18<=k<=18, -22<=l<=22
Reflections collected	32067
Independent reflections	7862 [R(int) = 0.0465]
Coverage of independent reflections	99.5%
Absorption correction	multi-scan
Max. and min. transmission	0.9000 and 0.4610
Structure solution technique	direct methods
Structure solution program	SHELXTL XT 2014/5 (Bruker AXS, 2014)
Refinement method	Full-matrix least-squares on F^2
Refinement program	SHELXTL XL 2018/3 (Bruker AXS, 2018)
Function minimized	$\Sigma\, w(F_o^2 - F_c^2)^2$
Data / restraints / parameters	7862 / 2 / 306
Goodness-of-fit on F^2	0.952
Δ/σ_{max}	0.001
Final R indices	7265 data; I>2σ(I) R1 = 0.0221, wR2 = 0.0406
	all data R1 = 0.0268, wR2 = 0.0416
Weighting scheme	$w=1/[\sigma^2(F_o^2)+(0.0012P)^2]$ where $P=(F_o^2+2F_c^2)/3$
Absolute structure parameter	0.005(6)
Largest diff. peak and hole	0.613 and -0.535 eÅ^{-3}
R.M.S. deviation from mean	0.096 eÅ^{-3}

Table S5. Sample and crystal data for **Os3.**

Chemical formula	$C_{36}H_{44}Os$
Formula weight	666.96 g/mol
Temperature	100(2) K
Wavelength	0.71073 Å
Crystal size	0.051 x 0.069 x 0.489 mm
Crystal habit	dark black rod
Crystal system	monoclinic
Space group	C 1 2/c 1
Unit cell dimensions	a = 16.265(3) Å
	b = 24.149(5) Å α = 90°
	c = 14.951(3) Å β = 93.736(3)°
Volume	5860.(2) $Å^3$ γ = 90°
Z	8
Density (calculated)	1.512 g/cm^3
Absorption coefficient	4.374 mm^{-1}
F(000)	2688

Table S6. Data collection and structure refinement for **Os3**.

Diffractometer	Bruker APEX II CCD Bruker APEX DUO
Radiation source	fine-focus tube (MoKα , λ = 0.71073 Å)
Theta range for data collection	1.51 to 27.48°
Index ranges	-21<=h<=21, -31<=k<=31, -19<=l<=19
Reflections collected	59569
Independent reflections	6726 [R(int) = 0.0501]
Coverage of independent reflections	99.9%
Absorption correction	multi-scan
Max. and min. transmission	0.8040 and 0.2230
Structure solution technique	direct methods
Structure solution program	SHELXTL XT 2014/5 (Bruker AXS, 2014)
Refinement method	Full-matrix least-squares on F^2
Refinement program	SHELXTL XL 2018/3 (Bruker AXS, 2018)
Function minimized	$\Sigma\, w(F_o^2 - F_c^2)^2$
Data / restraints / parameters	6726 / 0 / 346
Goodness-of-fit on F^2	1.160
Δ/σ_{max}	0.005
Final R indices	5752 data; I>2σ(I) R1 = 0.0257, wR2 = 0.0621
	all data R1 = 0.0333, wR2 = 0.0676
Weighting scheme	$w=1/[\sigma^2(F_o^2)+(0.0244P)^2+29.8209P]$ where $P=(F_o^2+2F_c^2)/3$
Largest diff. peak and hole	1.992 and -1.230 eÅ^{-3}
R.M.S. deviation from mean	0.124 eÅ^{-3}

Geometry Analysis

We apply **Equation S1** to calculate the "tetrahedricity"-value (*T*-value) for different tetrahedral compounds (compiled in **Table 1**), adapting an approach used by others to calculate the "octahedricity"-value (*O*-value) for a series of polypyridyl complexes.[22–24] The *T*-value is the root-mean-square deviation of a set of C–M–C angles from their ideal tetrahedral values (109.5°). The larger the *T*-value the greater the deviation of C-M-C angles from ideal and the more distorted the tetrahedral geometry, where a *T*-value = 0 indicates no deviation and a perfect tetrahedral geometry. Here, $\hat{\theta}_i$ = 109.5° for ideal C-M-C angles, and θ_i = the 6 unique experimental C-M-C angles determined from structural data. These unique angles are given for each compound in **Tables S8-S20**.

$$T\text{-value} = \sqrt{\frac{1}{6}\sum_{i=1}^{6}(\hat{\theta}_i - \theta_i)^2} \qquad \textbf{(S1)}$$

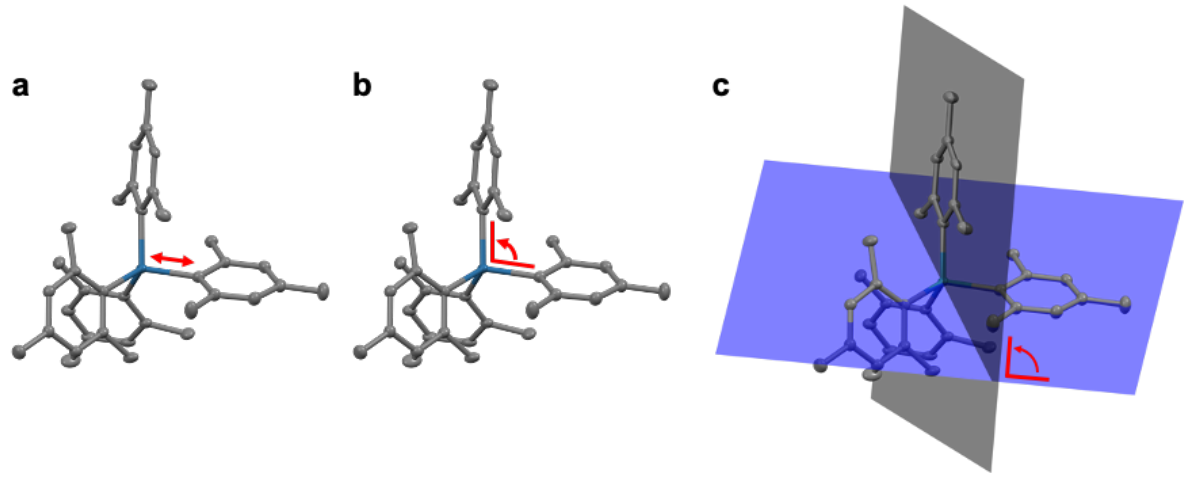

Figure S2. Illustrative definitions of selected structural parameters (red arrows) using the ellipsoid structure of **Os3** (Os = teal, C = grey). **(a)** M–C bond length, **(b)** C-M-C angle, and **(c)** aryl plane angle. Hydrogen atoms are omitted for clarity.

Table S7. Overview of additional structural parameters for selected compounds.[a]

			aryl plane (°)	
compound	M-C (Å)	C-M-C (°)	min-max	average
Os(mesityl)$_4$ (**Os3**)	2.026(3)-2.049(3)	98.4(1)-117.2(1)	63.93-82.89	70.49
Os(cyclohexyl)$_4$	2.026-2.031	105.4-117.1	-	-
Os(2-tolyl)$_4$ (**Os1**)	1.984-2.011	106.1-117.1	66.46-73.97	70.49
Os(4-Br-2,5-xylyl)$_4$	1.98(2)-2.03(3)	107.3(6)-111.6(7)	60.01-84.88	70.50
Os(phenyl)$_4$	1.995	107.6-110.4	62.04-86.44	70.17
Os(2,5-xylyl)$_4$ (**Os2**)	2.003(4)-2.017(4)	108.1(2)-110.9(2)	50.85-87.62	67.45
Ru(mesityl)$_4$ (**Ru3**)	2.00(1)-2.02(1)	99.1(4)-117.0(4)	64.25-81.47	70.51
Ru(cyclohexyl)$_4$	2.018-2.020	105.4-116.3	-	-
Ru(2-tolyl)$_4$ (**Ru1**)	1.943-2.047	106.3-114.9	64.83-77.36	70.46
Ru(4-MeO-2-tolyl)$_4$	1.986	106.0-111.2	61.39-87.58	70.12
Ru(4-Br-2,5-xylyl)$_4$	1.984	106.4-111.0	61.83-86.80	70.15
Ru(2,4,5-trimethylphenyl)$_4$	1.99-2.03	108.4-110.7	60.21-81.20	70.50
C(phenyl)$_4$	1.551	106.7-110.9	68.51-74.49	70.50

[a] Minimum and maximum values are provided to give an indication of range. Selected parameters are provided with estimated standard deviations (ESDs) in parentheses for all structures with associated ESDs. All bond lengths and angles used are tabulated in **Tables S8-S20**. For structure identifiers and references see **Table 1**. M = Os, Ru, C.

Table S8. Selected structural parameters for Os(mesityl)$_4$ (**Os3**).[a]

M-C bond length (Å)		C-M-C angle (°)		aryl plane angle (°)	
Os1-C1	2.049(3)	C1-Os1-C10	113.8(1)	(C1-C9)-(C10-C18)	67.00
Os1-C10	2.026(3)	C1-Os1-C19	98.4(1)	(C1-C9)-(C19-C27)	74.34
Os1-C19	2.038(3)	C1-Os1-C28	117.1(1)	(C1-C9)-(C28-C36)	63.92
Os1-C28	2.033(3)	C10-Os1-C19	117.2(1)	(C10-C18)-(C19-C27)	65.59
		C10-Os1-C28	98.7(1)	(C10-C18)-(C28-C36)	82.89
		C19-Os1-C28	112.8(1)	(C19-C27)-(C28-C36)	69.20

[a] Atom labels refer to deposited crystal structure labels. Selected parameters are provided with ESDs in parentheses. For structure identifier and reference see **Table 1**.

Table S9. Selected structural parameters for Os(cyclohexyl)$_4$.[a]

M-C bond length (Å)		C-M-C angle (°)	
Os1-C1	2.026	C1-Os1-C1B	117.1
Os1-C1B	2.026	C1-Os1-C7	106.3
Os1-C7	2.031	C1-Os1-C7B	105.4
Os1-C7B	2.031	C1B-Os1-C7	106.4
		C1B-Os1-C7B	106.3
		C7-Os1-C7B	117.0

[a] Atom labels refer to deposited crystal structure labels. For structure identifier and reference see **Table 1**.

Table S10. Selected structural parameters for Os(2-tolyl)$_4$ (**Os1**).[a]

M-C bond length (Å)		C-M-C angle (°)		aryl plane angle (°)	
Os1-C1	2.0106	C1-Os1-C1C	114.11	(C1-C6)-(C8-C13)	66.46
Os1-C1C	2.0106	C1-Os1-C8	106.06	(C1-C6)-(C1C-C6C)	73.97
Os1-C8	1.9835	C1-Os1-C8C	106.94	(C1-C6)-(C8C-C13C)	69.47
Os1-C8C	1.9835	C8-Os1-C8C	117.05	(C8-C13)-(C1C-C6C)	69.47
		C8-Os1-C1C	106.94	(C8-C13)-(C8C-C13C)	77.12
		C8C-Os1-C1C	106.06	(C1C-C6C)-(C8C-C13C)	66.46

[a] Atom labels refer to deposited crystal structure labels. For structure identifier and reference see **Table 1**.

Table S11. Selected structural parameters for Os(4-Br-2,5-xylyl)$_4$.[a]

M-C bond length (Å)		C-M-C angle (°)		aryl plane angle (°)	
Os1-C1	1.98(2)	C1-Os1-C9	107.3(6)	(C1-C8)-(C9-C16)	77.39
Os1-C9	2.00(2)	C1-Os1-C17	111.6(7)	(C1-C8)-(C17-C24)	60.01
Os1-C17	2.03(3)	C1-Os1-C25	109.4(7)	(C1-C8)-(C25-C32)	74.13
Os1-C28	1.99(2)	C-Os1-C17	110.7(6)	(C9-C16)-(C17-C24)	63.17
		C9-Os1-C25	110.3(6)	(C9-C16)-(C25-C32)	63.40
		C17-Os1-C25	107.5(6)	(C17-C24)-(C25-C32)	84.88

[a] Atom labels refer to deposited crystal structure labels. Selected parameters are provided with ESDs in parentheses. For structure identifier and reference see **Table 1**.

Table S12. Selected structural parameters for Os(phenyl)$_4$.[a]

M-C bond length (Å)		C-M-C angle (°)		aryl plane angle (°)	
Os1-C6	1.995	C6-Os1-C6A	110.4	(C1-C6)-(C1A-C6A)	62.04
Os1-C6A	1.995	C6-Os1-C6B	107.6	(C1-C6)-(C1B-C6B)	86.44
Os1-C6B	1.995	C6-Os1-C6C	110.4	(C1-C6)-(C1C-C6C)	62.04
Os1-C6C	1.995	C6A-Os1-C6B	110.4	(C1A-C6A)-(C1B-C6B)	62.04
		C6A-Os1-C6C	107.6	(C1A-C6A)-(C1C-C6C)	86.44
		C6B-Os1-C6C	110.4	(C1B-C6B)-(C1C-C6C)	62.04

[a] Atom labels refer to deposited crystal structure labels. For structure identifier and reference see **Table 1**.

Table S13. Selected structural parameters for Os(2,5-xylyl)$_4$ (**Os2**).[a]

M-C bond length (Å)		C-M-C angle (°)		aryl plane angle (°)	
Os1-C1	2.003(4)	C1-Os1-C9	108.1(2)	(C1-C8)-(C9-C16)	61.93
Os1-C9	2.017(4)	C1-Os1-C17	108.6(2)	(C1-C8)-(C17-C24)	50.85
Os1-C17	2.005(5)	C1-Os1-C25	109.5(2)	(C1-C8)-(C25-C32)	85.02
Os1-C28	2.006(4)	C9-Os1-C17	108.7(2)	(C9-C16)-(C17-C24)	87.62
		C9-Os1-C25	110.9(2)	(C9-C16)-(C25-C32)	61.51
		C17-Os1-C25	110.9(2)	(C17-C24)-(C25-C32)	57.75

[a] Atom labels refer to deposited crystal structure labels. Selected parameters are provided with ESDs in parentheses. For structure identifier and reference see **Table 1**.

Table S14. Selected structural parameters for Ru(mesityl)$_4$ (**Ru3**).[a]

M-C bond length (Å)		C-M-C angle (°)		aryl plane angle (°)	
Ru1-C1	2.00(1)	C1-Ru1-C7	113.6(4)	(C1-C6)-(C7-C12)	66.99
Ru1-C7	2.02(1)	C1-Ru1-C13	99.6(4)	(C1-C6)-(C13-C18)	81.47
Ru1-C13	2.01(1)	C1-Ru1-C19	116.0(4)	(C1-C6)-(C19-C24)	66.59
Ru1-C19	2.01(1)	C7-Ru1-C13	117.0(4)	(C7-C12)-(C13-C18)	64.25
		C7-Ru1-C19	99.1(4)	(C7-C12)-(C19-C24)	73.80
		C13-Ru1-C19	112.5(4)	(C13-C18)-(C19-C24)	69.96

[a] Atom labels refer to deposited crystal structure labels. Selected parameters are provided with ESDs in parentheses. For structure identifier and reference see **Table 1**.

Table S15. Selected structural parameters for Ru(cyclohexyl)$_4$.[a]

M-C bond length (Å)		C-M-C angle (°)	
Ru1-C1	2.020	C1-Ru1-C1B	116.3
Ru1-C1B	2.020	C1-Ru1-C7	107.1
Ru1-C7	2.018	C1-Ru1-C7B	105.4
Ru1-C7B	2.018	C1B-Ru1-C7	105.4
		C1B-Ru1-C7B	107.1
		C7-Ru1-C7B	107.1

[a] Atom labels refer to deposited crystal structure labels. For structure identifier and reference see **Table 1**.

Table S16. Selected structural parameters for Ru(2-tolyl)$_4$ (**Ru1**).[a]

M-C bond length (Å)		C-M-C angle (°)		aryl plane angle (°)	
Ru1-C1	2.047	C1-Ru1-C1C	114.9	(C1-C6)-(C8-C13)	70.24
Ru1-C1C	2.047	C1-Ru1-C8	106.3	(C1-C6)-(C1C-C6C)	75.28
Ru1-C8	1.943	C1-Ru1-C8C	107.8	(C1-C6)-(C8C-C13C)	64.83
Ru1-C8C	1.943	C8-Ru1-C1C	107.8	(C8-C13)-(C1C-C6C)	64.83
		C8-Ru1-C8C	113.9	(C8-C13)-(C8C-C13C)	77.36
		C8C-Ru1-C1C	106.3	(C1C-C6C)-(C8C-C13C)	70.24

[a] Atom labels refer to deposited crystal structure labels. For structure identifier and reference see **Table 1**.

Table S17. Selected structural parameters for Ru(4-MeO-2-tolyl)$_4$.[a]

M-C bond length (Å)		C-M-C angle (°)		aryl plane angle (°)	
Ru1-C1	1.986	C1-Ru1-C1	111.2	(C1-C6)-(C6-C1)	61.39
Ru1-C1	1.986	C1-Ru1-C1	111.2	(C1-C6)-(C6-C1)	87.58
Ru1-C1	1.986	C1-Ru1-C1	106.0	(C1-C6)-(C6-C1)	61.39
Ru1-C1	1.986	C1-Ru1-C1	106.0	(C1-C6)-(C6-C1)	61.39
		C1-Ru1-C1	111.2	(C1-C6)-(C6-C1)	61.39
		C1-Ru1-C1	111.2	(C1-C6)-(C6-C1)	87.58

[a] Atom labels refer to deposited crystal structure labels. For structure identifier and reference see **Table 1**.

Table S18. Selected structural parameters for Ru(4-Br-2,5-xylyl)$_4$.[a]

M-C bond length (Å)		C-M-C angle (°)		aryl plane angle (°)	
Ru1-C1	1.984	C1-Ru1-C1	111.0	(C1-C6)-(C6-C1)	61.83
Ru1-C1	1.984	C1-Ru1-C1	111.0	(C1-C6)-(C6-C1)	86.80
Ru1-C1	1.984	C1-Ru1-C1	106.4	(C1-C6)-(C6-C1)	61.83
Ru1-C1	1.984	C1-Ru1-C1	111.0	(C1-C6)-(C6-C1)	86.80
		C1-Ru1-C1	106.4	(C1-C6)-(C6-C1)	61.83
		C1-Ru1-C1	111.0	(C1-C6)-(C6-C1)	61.83

[a] Atom labels refer to deposited crystal structure labels. Estimated standard deviations shown in brackets where applicable. For structure identifier and reference see **Table 1**.

Table S19. Selected structural parameters for Ru(2,4,5-trimethylphenyl)$_4$.[a]

M-C bond length (Å)		C-M-C angle (°)		aryl plane angle (°)	
Ru1-C11	2.03(1)	C11-Ru1-C21	109.4(5)	(C11-C16)-(C21-C26)	81.20
Ru1-C21	2.00(1)	C11-Ru1-C31	108.7(5)	(C11-C16)-(C31-C36)	70.92
Ru1-C31	1.92(1)	C11-Ru1-C41	110.5(4)	(C11-C16)-(C41-C46)	67.64
Ru1-C41	1.99(1)	C21-Ru1-C31	110.7(5)	(C21-C26)-(C31-C36)	60.21
		C21-Ru1-C41	109.2(5)	(C21-C26)-(C41-C46)	67.33
		C31-Ru1-C41	108.4(4)	(C31-C36)-(C41-C46)	75.72

[a] Atom labels refer to deposited crystal structure labels. Selected parameters are provided with ESDs in parentheses. For structure identifier and reference see **Table 1**.

Table S20. Selected structural parameters for tetraphenylmethane, C(phenyl)$_4$.[a]

C-C bond length (Å)		C-M-C angle (°)		aryl plane angle (°)	
C7-C1	1.5509	C1-C7-C1	110.86	(C1-C6)-(C6-C1)	68.51
C7-C1	1.5509	C1-C7-C1	106.72	(C1-C6)-(C6-C1)	68.51
C7-C1	1.5509	C1-C7-C1	110.86	(C1-C6)-(C6-C1)	74.49
C7-C1	1.5509	C1-C7-C1	106.72	(C1-C6)-(C6-C1)	68.51
		C1-C7-C1	110.86	(C1-C6)-(C6-C1)	68.51
		C1-C7-C1	110.86	(C1-C6)-(C6-C1)	74.49

[a] Atom labels refer to deposited crystal structure labels. For structure identifier and reference see **Table 1**.

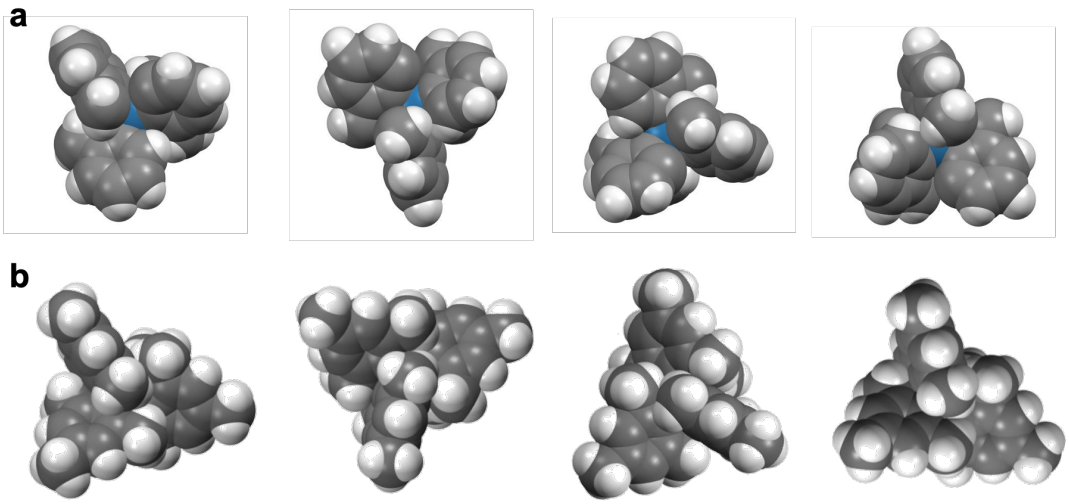

Figure S3. Space filling models of **(a) Os1**[10] and **(b) Os3**, viewed along each Os-C axis, illustrating the additional steric shielding conferred by the second *ortho*-methyl group in **Os3** (Os = teal, C = grey, H = white).

4. Electrochemistry

Table S21. Electrochemical data for Os(aryl)$_4$ complexes.[a]

	redox transition	E_{pa} (V)	E_{pc} (V)	ΔE	i_{pa}/i_{pc}
Os(2-tolyl)$_4$ (**Os1**)	1−/0	−1.918	−2.004	0.086	0.97
	0/1+	0.366	0.287	0.079	0.98
Os(2,5-xylyl)$_4$ (**Os2**)	1−/0	−1.969	−2.047	0.078	0.98
	0/1+	0.281	0.208	0.073	1.00
Os(mesityl)$_4$ (**Os3**)	1−/0	−1.992	−2.064	0.072	0.98
	0/1+	0.187	0.120	0.067	1.00
	1+/2+	1.155	1.079	0.076	1.12 [b]

[a] Scan rate = 0.1 V s^{-1}; NBu_4PF_6 supporting electrolyte; working electrode: glassy carbon; reference electrode, counter electrode: Pt. All potentials corrected for iR_u and reported relative to $[Cp_2Fe]^+/Cp_2Fe$. [b] Redox feature overlap with onset of solvent oxidation makes it difficult to define peak baselines and accurately determine i_{pa}/i_{pc}. Overlaid cyclic voltammograms for **Os3** recorded at different scan rates are presented in **Figure S4**.

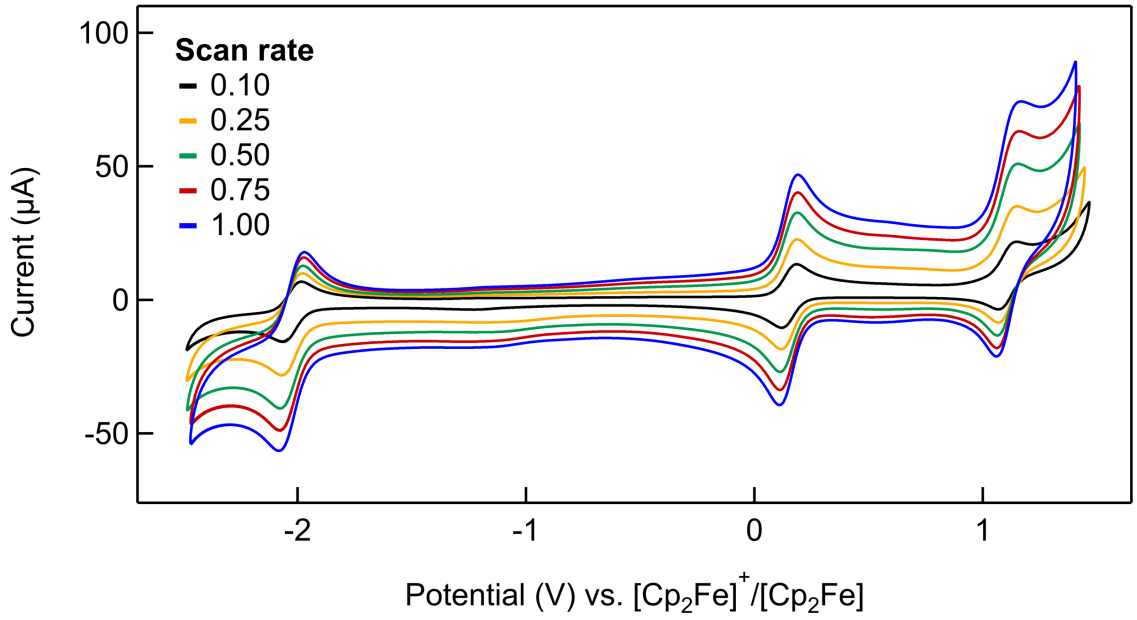

Figure S4. Overlaid voltammograms showing the dependence of current on scan rate for Os(mesityl)$_4$ (**Os3**). Potentials are reported relative to $[Cp_2Fe]^+/[Cp_2Fe]$, corrected for iR_u. For conditions see main text.

5. NMR Spectra

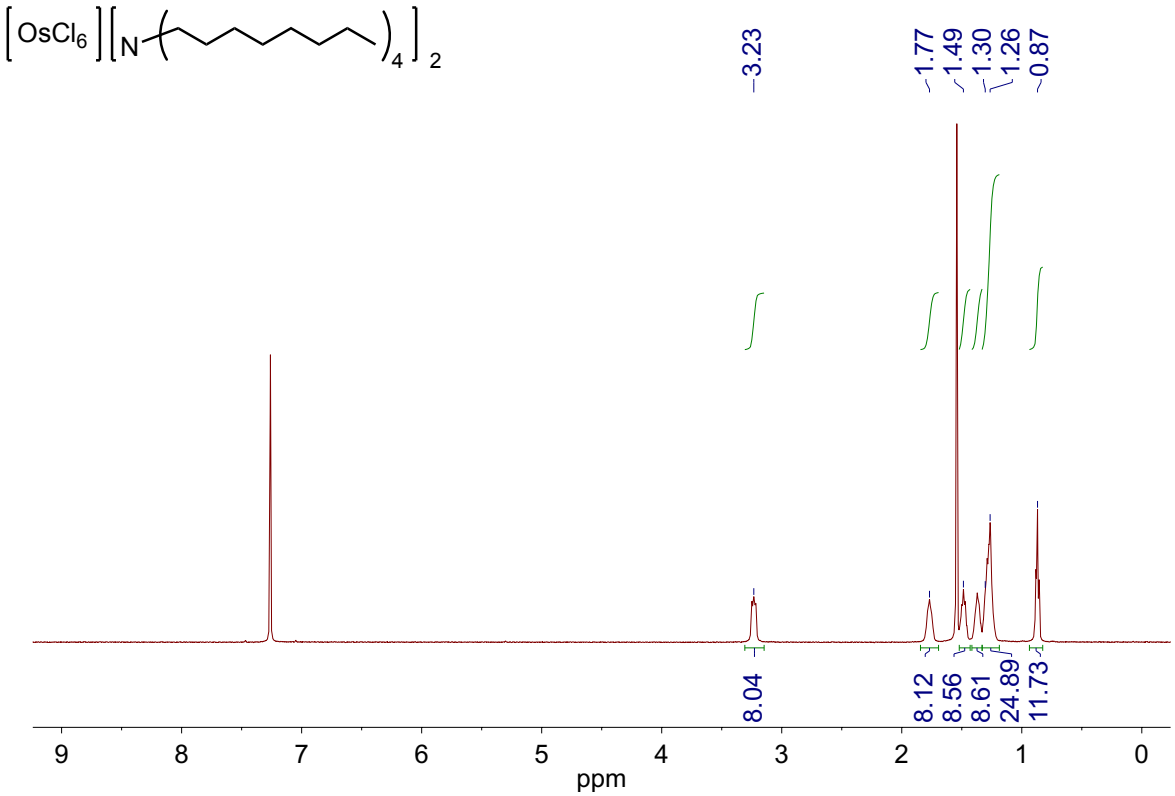

Figure S5. ^{1}H NMR spectra of $(Oct_4N)_2[OsCl_6]$ in $CDCl_3$.

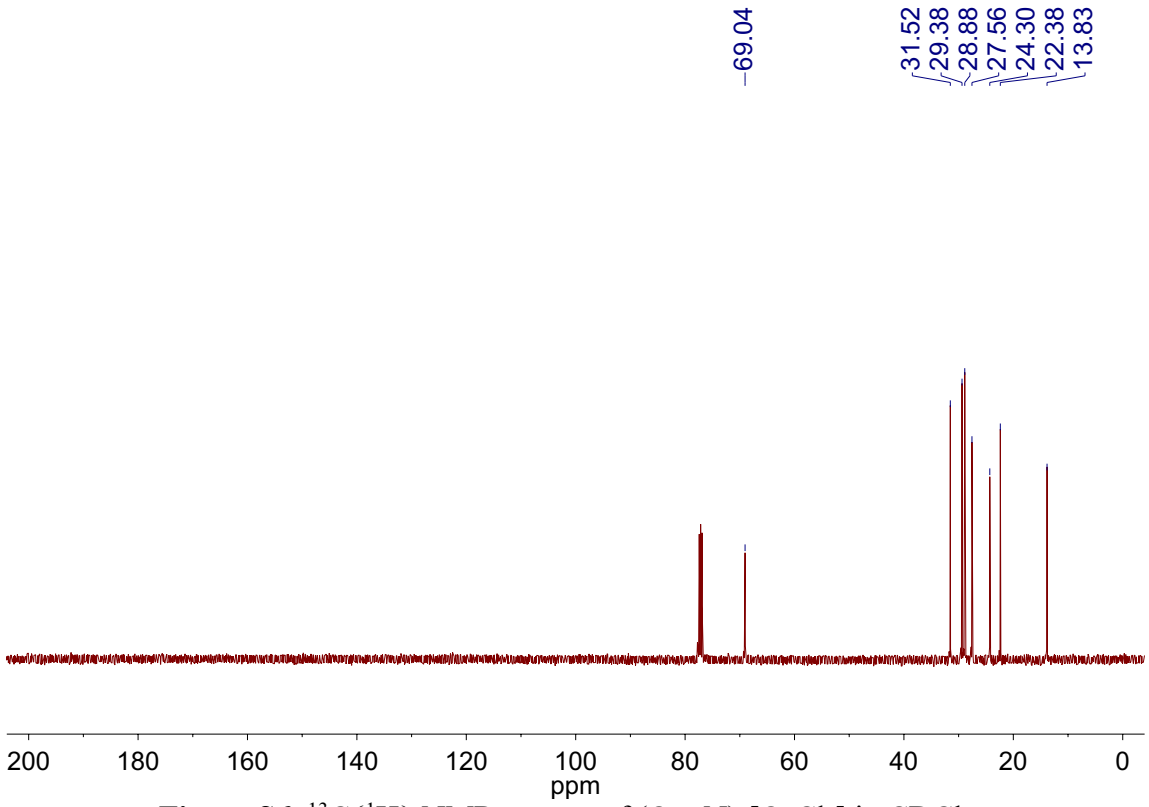

Figure S6. $^{13}C\{^{1}H\}$ NMR spectra of $(Oct_4N)_2[OsCl_6]$ in $CDCl_3$.

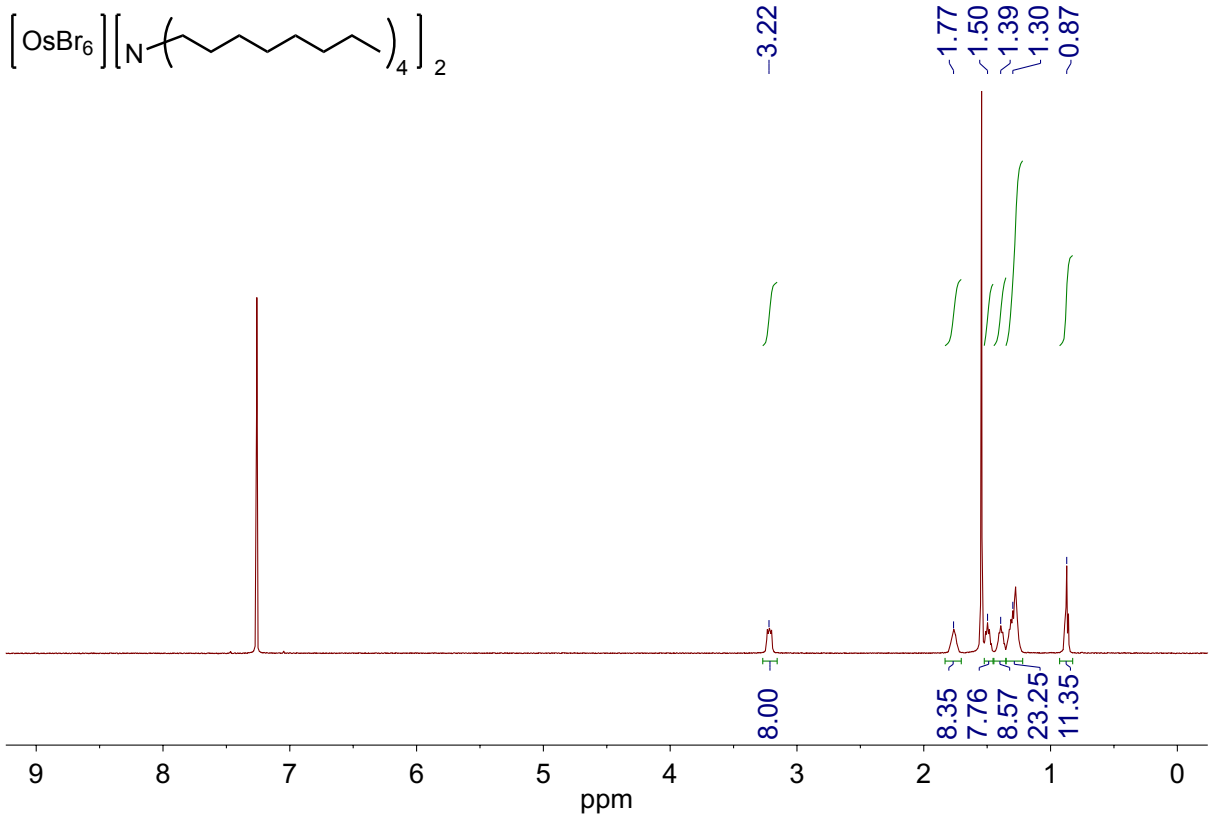

Figure S7. ^{1}H NMR spectra of $(Oct_4N)_2[OsBr_6]$ in $CDCl_3$.

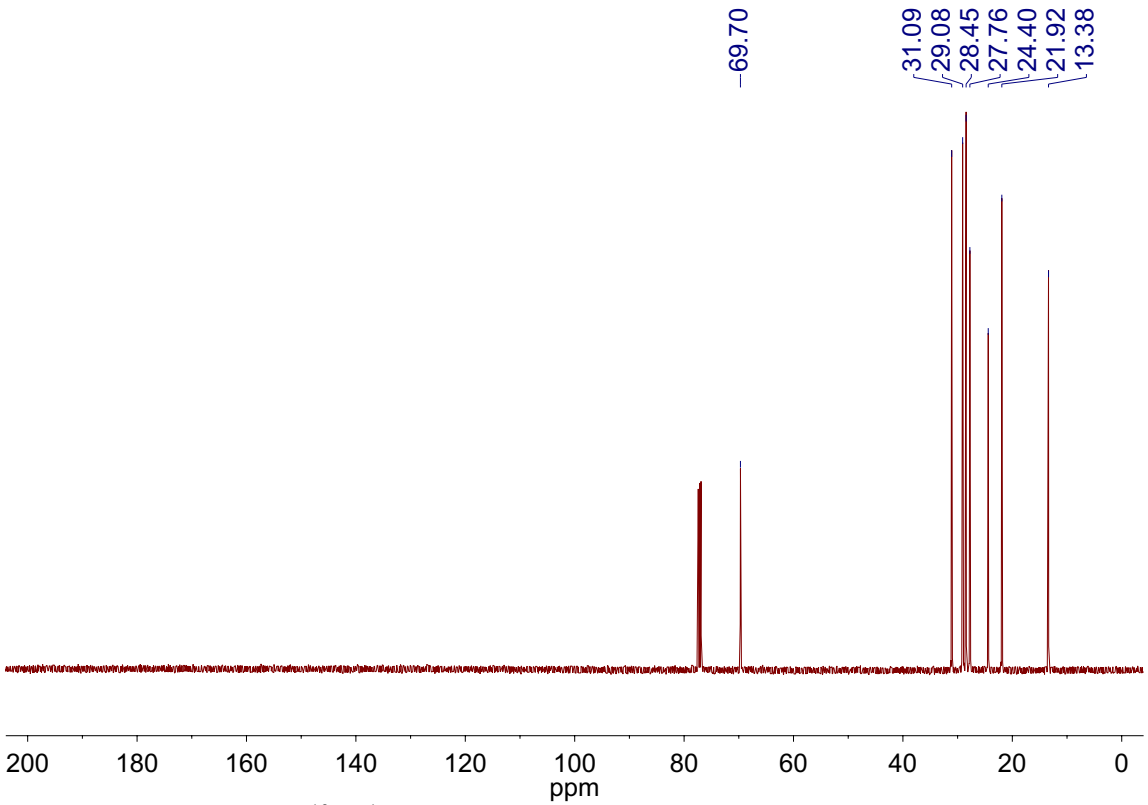

Figure S8. $^{13}C\{^{1}H\}$ NMR spectra of $(Oct_4N)_2[OsBr_6]$ in $CDCl_3$.

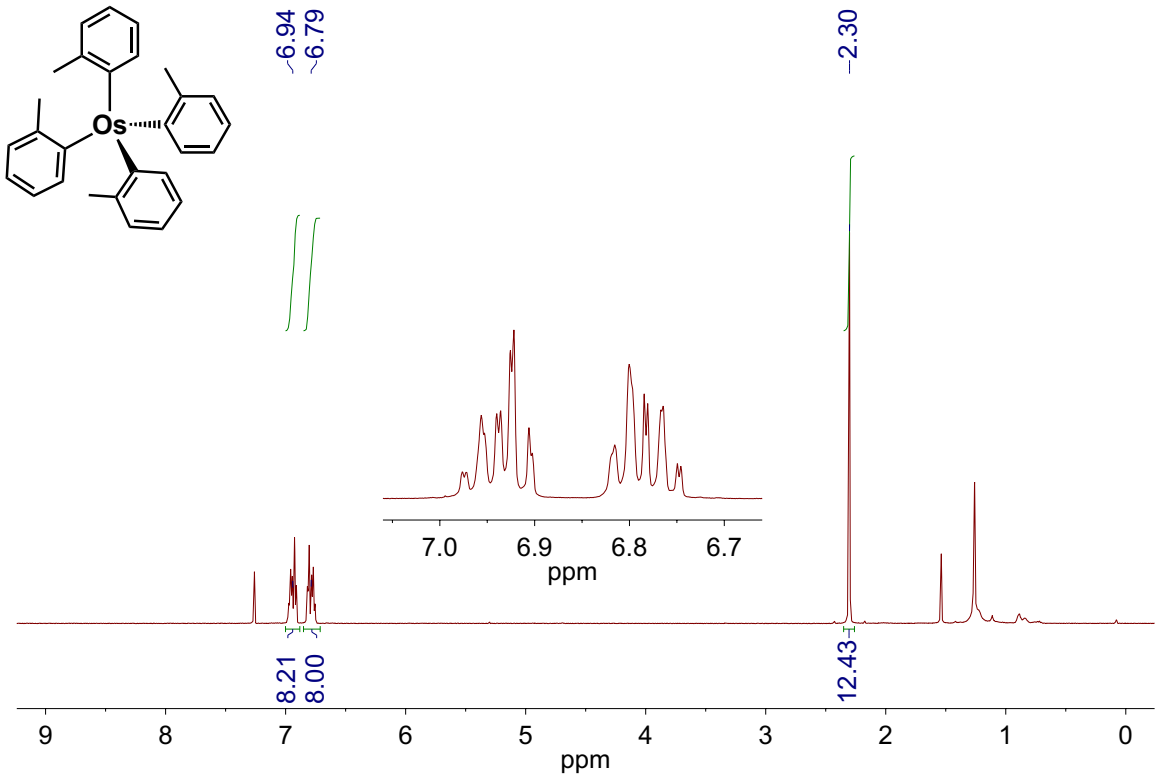

Figure S9. ^{1}H NMR spectra of Os(2-tolyl)$_4$ **(Os1)** in $CDCl_3$.

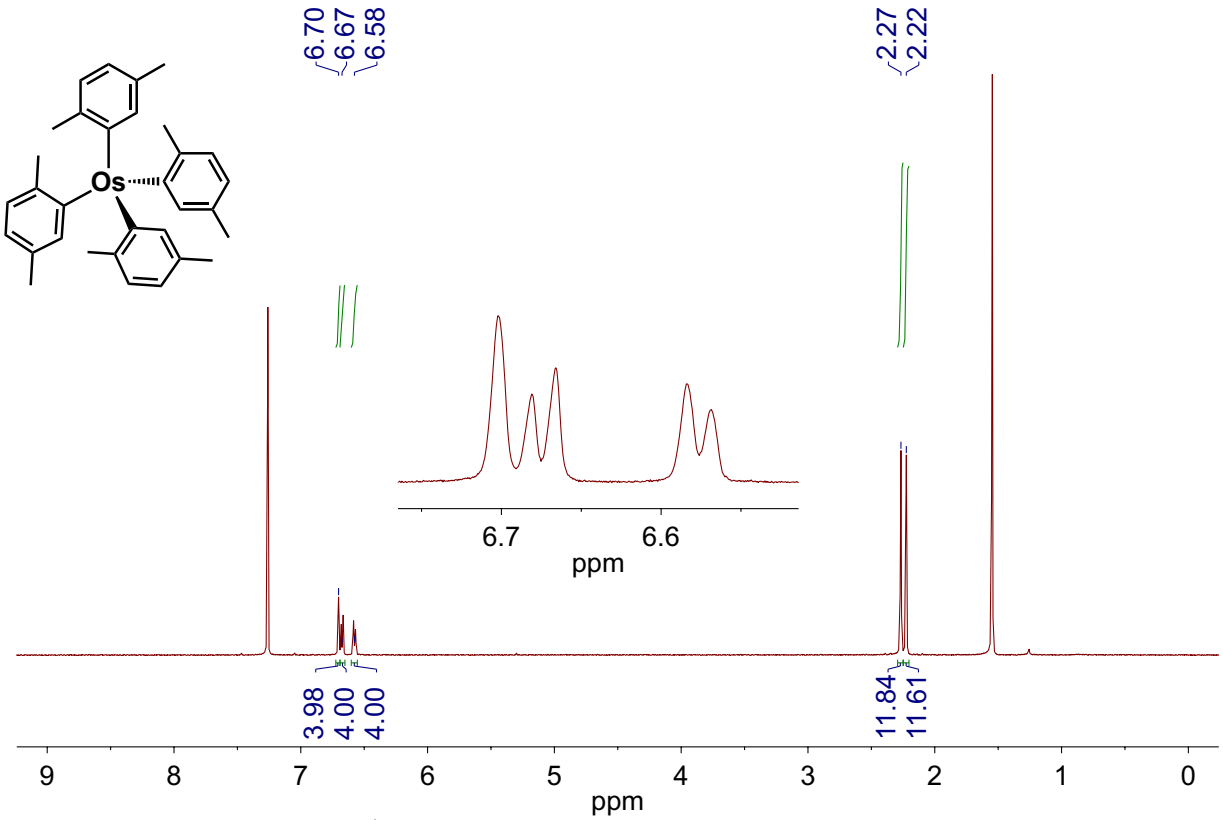

Figure S10. ^{1}H NMR spectra of Os(2,5-xylyl)$_4$ **(Os2)** in $CDCl_3$.

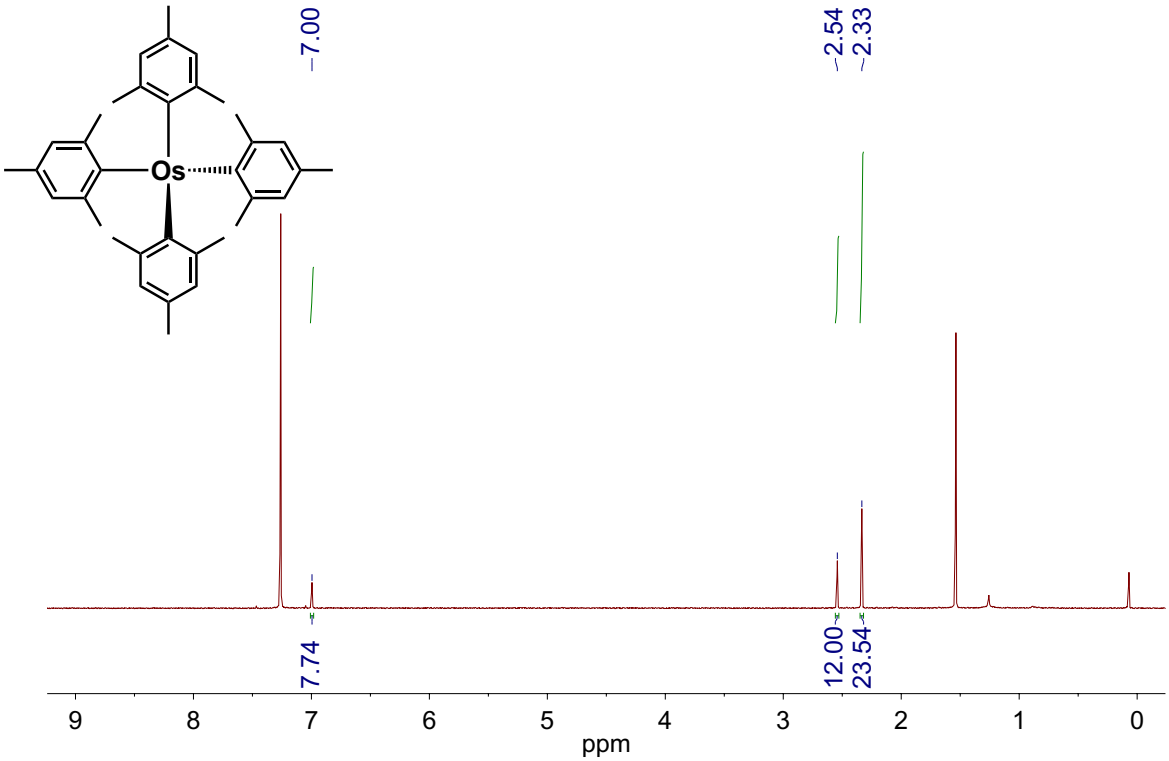

Figure S11. ^{1}H NMR spectra of Os(mesityl)$_4$ **(Os3)** in $CDCl_3$.

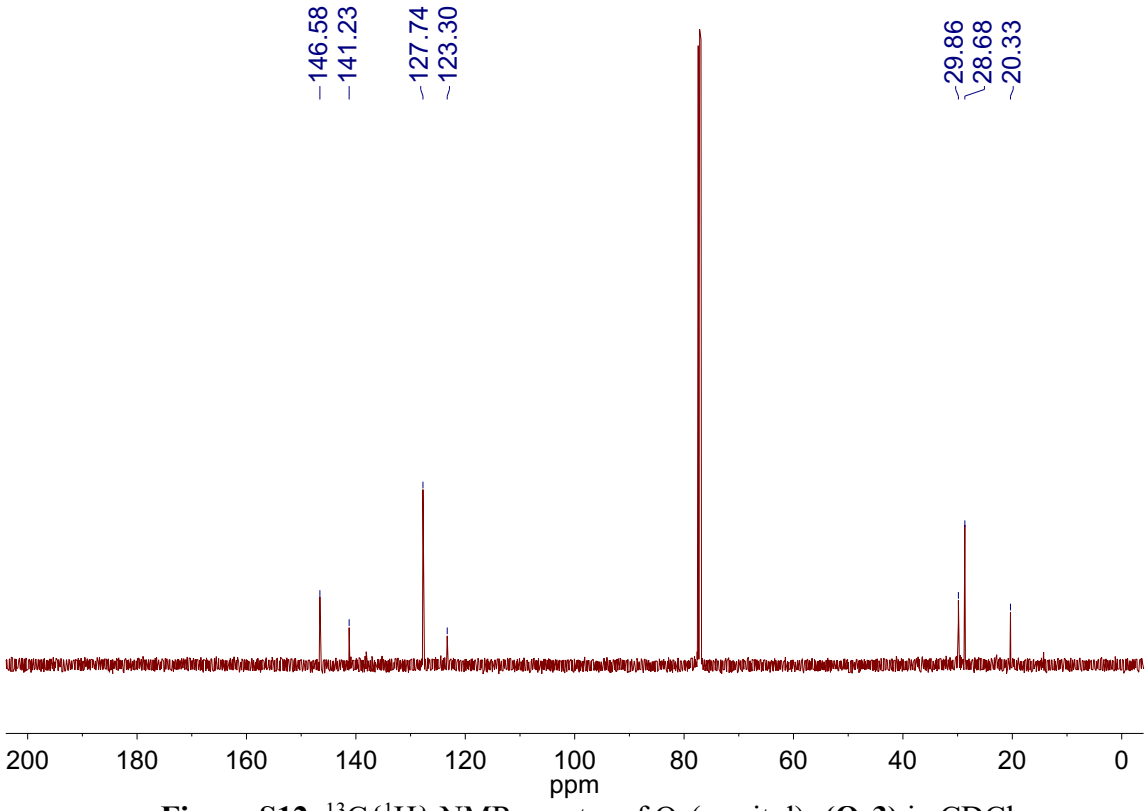

Figure S12. $^{13}C\{^{1}H\}$ NMR spectra of Os(mesityl)$_4$ **(Os3)** in $CDCl_3$.

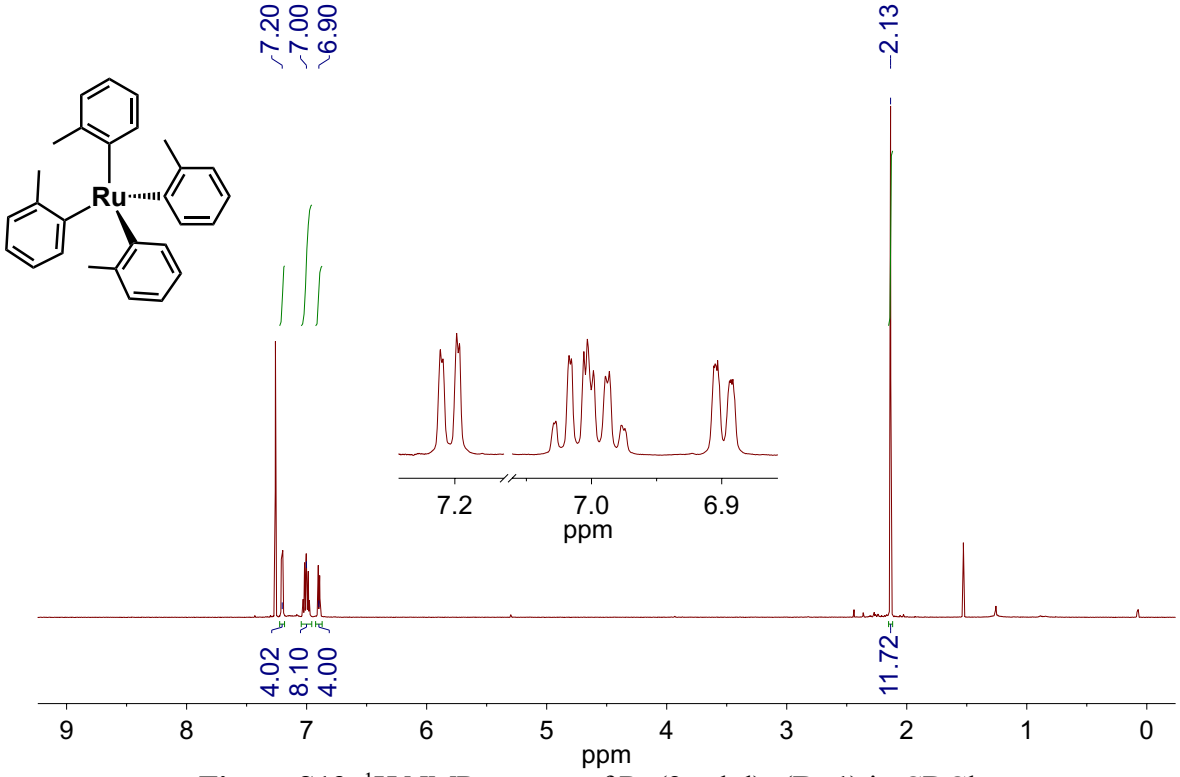

Figure S13. ^{1}H NMR spectra of Ru(2-tolyl)$_4$ (**Ru1**) in $CDCl_3$.

6. References

1 B. E. Love and E. G. Jones, *J. Org. Chem.*, 1999, **64**, 3755–3756.

2 J. R. Rodriguez, R. M. Félix, E. A. Reynoso, S. Fuentes Moyado and G. Alonso-Núñez, *Inorganica Chim. Acta*, 2013, **406**, 138–145.

3 F. P. Dwyer, J. W. Hogarth and R. N. Rhoda, in *Inorg. Synth.*, ed. T. Moeller, 1957, vol. 5, pp. 206–207.

4 F. P. Dwyer, J. W. Hogarth and R. N. Rhoda, in *Inorg. Synth.*, ed. T. Moeller, 1957, vol. 5, pp. 204–206.

5 G. R. Fulmer, A. J. M. Miller, N. H. Sherden, H. E. Gottlieb, A. Nudelman, B. M. Stoltz, J. E. Bercaw and K. I. Goldberg, *Organometallics*, 2010, **29**, 2176–2179.

6 P. D. Savage, G. Wilkinson, M. Motevalli and M. B. Hursthouse, *J. Chem. Soc., Dalt. Trans.*, 1988, 669–673.

7 C.-J. Wang, X.-L. Wu, X.-F. Ma, A.-Q. Jia and Q.-F. Zhang, *Z. Naturforsch*, 2017, **72**, 523–525.

8 S. C. So, W. M. Cheung, G. C. Wang, E. Kwan Huang, M. K. Lau, Q. F. Zhang, H. H. Y. Sung, I. D. Williams and W. H. Leung, *Organometallics*, 2014, **33**, 4497–4502.

9 R. Hay-Motherwell, G. Wilkinson, B. Hussain-Bates and M. Hurthouse, *Dalton Trans.*, 1992, 3477–3482.

10 R. P. Tooze, P. Stavropoulos, M. Motevalli, M. B. Hursthouse and G. Wilkinson, *J. Chem. Soc. Chem. Commun.*, 1985, **0**, 1139–1140.

11 D. T. Hardy, G. Wilkinson and G. B. Young, *Polyhedron*, 1996, **15**, 1363–1373.

12 M.-K. Lau, J. L. Chim, W.-T. Wong, I. D. Williams and W.-H. Leung, *Can. J. Chem.*, 2001, **79**, 607–612.

13 P. Stravropoulos, P. G. Edwards, T. Behling, G. Wilkinson, M. Motevalli and M. B. Hursthouse, *J. Chem. Soc. Dalt. Trans.*, 1987, 169–175.

14 P. Stavropoulos, P. D. Savage, R. P. Tooze, G. Wilkinson, B. Hussain, M. Motevalli and M. B. Hursthouse, *J. Chem. Soc. Dalt. Trans.*, 1987, 557–562.

15 C. J. Longley, P. D. Savage, G. Wilkinson, B. Hussain and M. Hurthouse, *Polyhedron*, 1988, **7**, 1079–88.

16 B. A. Murrer, WO Pat., 10177, 1991.

17 P. Stavropoulos, P. D. Savage, R. P. Tooze, G. Wilkinson, B. Hussain, M. Motevalli and M. B. Hursthouse, *J. Chem. Soc. Dalt. Trans.*, 1987, 557–562.

18 SHELXTL 2014/7, Bruker AXS, Madison, WI, 2014.

19 G. M. Sheldrick, *Acta Crystallogr., Sect. A*, 2008, **64**, 112–122.

20 G. M. Sheldrick, *Acta Crystallogr., Sect. C*, 2015, **71**, 3–8.

21 C. B. Hübschle, G. M. Sheldrick and B. Dittrich, *J. Appl. Crystallogr.*, 2011, **44**, 1281–1284.

22 C. M. Brown, N. E. Arsenault, T. N. K. Cross, D. Hean, Z. Xu and M. O. Wolf, *Inorg. Chem. Front.*, 2020, **7**, 117–127.

23 T. Österman, M. Abrahamsson, H.-C. Becker, L. Hammarström and P. Persson, *J. Phys. Chem. A*, 2012, **116**, 1041–1050.

24 M. J. Lundqvist, Ph.D. thesis, Uppsala University, 2006.